

Oxygenated Metabolites of Anandamide and 2-Arachidonoylglycerol: Conformational Analysis and Interaction with Cannabinoid Receptors, Membrane Transporter, and Fatty Acid Amide Hydrolase

Mario van der Stelt,[†] J. Albert van Kuik,[†] Monica Bari,[‡] Guus van Zadelhoff,[†] Bas R. Leeflang,[†] Gerrit A. Veldink,^{*,†} Alessandro Finazzi-Agrò,[‡] Johannes F. G. Vliegthart,[†] and Mauro Maccarrone^{*,‡}

Department of Bio-organic Chemistry, Bijvoet Center for Biomolecular Research, Utrecht University, The Netherlands, and Department of Experimental Medicine and Biochemical Sciences, University of Rome "Tor Vergata", Rome, Italy

Received January 9, 2002

This study was aimed at finding structural requirements for the interaction of the acyl chain of endocannabinoids with cannabinoid receptors, membrane transporter protein, and fatty acid amide hydrolase (FAAH). To this end, the flexibility of the acyl chain was restricted by introduction of an 1-hydroxy-2Z,4E-pentadiene system in anandamide (*N*-arachidonoyl ethanolamine, AEA) and 2-arachidonoylglycerol (2-AG) at various positions using different lipoxygenases. This brought about selectivity and attenuated the binding potency of AEA and 2-AG. Although the displacement constants were modest, 15(*S*)-hydroxy-eicosa-5Z,8Z,11Z,13E-tetraenoyl-*N*-(2-hydroxyethyl)amine was found to bind selectively to the CB₁ receptor, whereas its 1-arachidonoyl-*sn*-glycerol analogue and 13(*S*)-hydroxy-octadeca-9Z,11E-dienoyl-*N*-(2-hydroxyethyl)amine could selectively bind to the CB₂ receptor. 11(*S*)-Hydroxy-eicosa-5Z,8Z,12E,14Z-tetraenoyl-*N*-(2-hydroxyethyl)amine did not bind to either receptor, whereas 12(*S*)-hydroxy-eicosa-5Z,8Z,10E,14Z-tetraenoyl-*N*-(2-hydroxyethyl)amine did bind to both CB receptors with an affinity similar to that of AEA. All oxygenated anandamide derivatives were good inhibitors of FAAH (low micromolar *K_i*) but were ineffective on the AEA transporter. 2-AG rapidly isomerizes into 1(3)-arachidonoyl-*sn*-glycerol. Both 1- and 3-arachidonoyl-*sn*-glycerol did not bind to either CB receptor and did not interfere with AEA transport. Thus, after it is isomerized, 2-AG is inactivated, thereby decreasing effective concentrations of 2-AG. Analysis of ¹H NMR spectra revealed that chloroform did not induce notably different conformations in the acyl chain of 15(*S*)-hydroxy-eicosa-5Z,8Z,11Z,13E-tetraenoic acid as compared with water. Molecular dynamics (MD) simulations of AEA and its analogues in the presence of explicit water molecules revealed that a tightly folded conformation of the acyl chain is not the only requirement for CB₁ binding. Structural details of the C₂–C₁₅ loop, such as an sp² carbon at position 11, are necessary for receptor binding. The MD simulations may suggest that the average orientations of the pentyl tail of AEA and 12(*S*)-hydroxy-eicosa-5Z,8Z,10E,14Z-tetraenoyl-*N*-(2-hydroxyethyl)amine are different from that of the low-affinity, inactive ligands.

Introduction

Anandamide (AEA; 5Z,8Z,11Z,14Z-eicosatetraenoyl-*N*-(2-hydroxyethyl)amine; arachidonoyl ethanolamide) is an endogenous lipid with neuro- and immunomodulatory activities. Many of the physiological activities of AEA are mediated via its interaction with cannabinoid CB₁ and CB₂ receptors, thereby mimicking some of the effects of Δ⁹-tetrahydrocannabinol (THC), the psychoactive compound in marijuana (Figure 1).^{1,2} AEA and 2-arachidonoylglycerol (2-AG) are the main endocannabinoids, i.e., endogenous ligands of the CB receptors.^{3–5} The effects of the endocannabinoids at the CB₁ and CB₂ receptors depend on the life span of these molecules in the extracellular space. AEA and 2-AG are inactivated by a rapid and selective process of transporter-mediated cellular uptake,⁶ followed by intracellular degradation

to arachidonic acid and ethanolamine or glycerol by the enzyme fatty acid amide hydrolase (FAAH).^{7,8} The endocannabinoid system, which constitutes the endocannabinoids, CB receptors, transporter protein, and FAAH, seems to be involved in the regulation of several physiological functions such as embryo implantation, pain, appetite, and blood pressure.^{9–12} Selective molecular probes targeted to one of the proteins of the endocannabinoid system are believed to yield useful therapeutics for a variety of disorders such as liver cirrhosis, multiple sclerosis, and obesity, as well as for several neurodegenerative diseases including stroke.^{13–19} To develop selective therapeutic agents, research is aimed at identifying essential structural properties of the endocannabinoids, which are needed for specific interactions with the CB receptors, AEA membrane transporter, and FAAH.^{15,20–22}

Crystal or NMR structures of any of the proteins of the endocannabinoid system might help to elucidate the nature of the ligand–protein interaction, but they are not yet available. Therefore, a structural comparison of

* To whom correspondence should be addressed. G.A.V.: Tel: + 31 30 2532661. Fax: + 31 30 2540980. E-mail: g.a.veldink@chem.uu.nl. M.M.: Tel: + 39 06 72 59 6388. Fax: + 39 06 72 59 64 68. E-mail: Maccarrone@med.uniroma2.it.

[†] Utrecht University.

[‡] University of Rome "Tor Vergata".

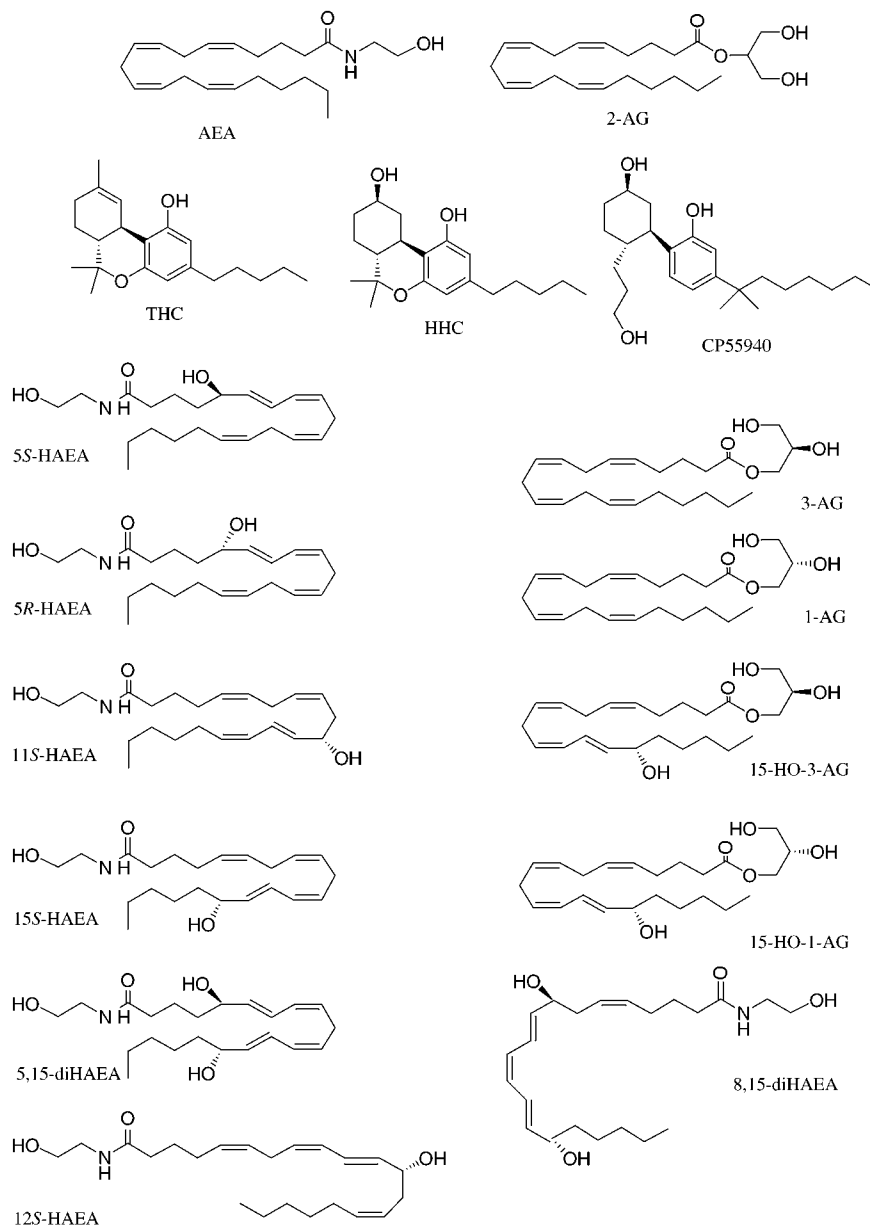


Figure 1. Chemical structures of classical, synthetic, and endogenous cannabinoids and their derivatives.

active and inactive classical and synthetic cannabinoids has been used to derive pharmacophore models.^{23–25} These models might also be used to predict and facilitate the design of novel compounds with greater potency or selectivity at the molecular target of interest.^{23–26} A prerequisite for the building of such a pharmacophore model is to characterize an ensemble of active conformations of a molecule. AEA can assume many different conformations, which originate primarily in its acyl chain. It has been suggested that a tightly folded conformation is responsible for the interaction of AEA with CB receptors.²⁰ However, this has not been substantiated as yet.

To get more insight into the structural requirements of the acyl chain of AEA to selectively interact with the proteins of the cannabinoid system and in particular the CB₁ receptor, we have combined interaction studies, ¹H NMR spectroscopy, and molecular dynamic (MD) simulations. The 1*Z*,4*Z*-pentadiene systems of the endocannabinoids were systematically converted into 1-hydroxy-

2*E*,4*Z*-pentadiene systems at different positions of the acyl chain by using different lipoxygenases as biocatalysts. We extended the studies of Hampson et al. and Edgemond et al. to other oxygenated metabolites to compare all derivatives in one system.^{27,28} CB₁ and CB₂ binding assays were performed as well as assays in which the effects of the oxygenated metabolites on AEA inactivation were studied. ¹H NMR was used to study the solvent effect on the conformation of the acyl chain. MD simulations of AEA and congeners with explicit water molecules were performed to determine the influence of conjugation of the double bond system on its conformation.

Results and Discussion

Interaction with CB₁ and CB₂ Receptors. In accordance with previous observations, AEA inhibited the specific binding of [³H]CP-55,940 to rat brain membranes, which express CB₁ receptors, in a manner typical of competing ligands with an inhibition constant

Table 1. Displacement Constants (K_i) of AEA and Their Oxygenated Metabolites for CB₁ and CB₂ Receptor Binding

compd	CB ₁ (nM) ^a	CB ₂ (nM) ^b	CB ₁ /CB ₂	literature values (nM)	
				CB ₁	CB ₂
AEA	90 ± 20	360 ± 50	0.36	71 ^c /107 ^d	94 ^e
5(S)-HAEA	>1000	>1000			
5(R)-HAEA	680 ± 140	710 ± 145	0.96		
11(S)-HAEA	>1000	>1000		1102 ^c	
11(R/S)-HAEA	>1000	>1000			
12(S)-HAEA	150 ± 30	500 ± 60	0.3	31 ^c /207 ^d	131 ^e
13(S)-HLEA	>1000	600 ± 120	1.7>		
15(S)-HAEA	600 ± 120	>1000	<0.6	418 ^c /738 ^d	1000 ^e >
15(R/S)-HAEA	680 ± 140	>1000	0.7>		
5,15-diHAEA	>1000	>1000			
8,15-diHAEA	>1000	>1000			

^a K_i values were calculated from the displacement curves of [³H]CP-55,940 from rat forebrain membranes in the presence of PMSF. ^b K_i values were calculated from the displacement curves of [³H]CP-55,940 from rat spleen membranes in the presence of PMSF. ^c K_i values were calculated from the displacement curves of [³H]CP-55,940 from rat brain synaptosomal membranes.²⁸ ^d K_i values were calculated from the displacement curves of [³H]CP-55,940 from rat forebrain membranes.²⁷ ^e K_i values were calculated from the displacement curves of [³H]CP-55,940 from human CB₂ receptor expressed in CHO cells.²⁷

of 90 nM (Table 1)² in the presence of PMSF. Compounds with a $K_i > 1 \mu\text{M}$ were considered inactive; therefore, an upper limit of $1 \mu\text{M}$ was set for binding potency.²⁹ Introduction of a hydroxyl function and a conjugated diene system in AEA by various lipoygenases reduced the capacity of AEA derivatives to compete for CB₁ binding (Table 1). Only 12*S*-HAEA retained a binding affinity in the same order of magnitude as AEA. 15*S*-HAEA and 5*R*-HAEA had a ~7-fold higher K_i , while 11*S*-HAEA, 5*S*-HAEA, and 13*S*-HLEA were inactive (Table 1). Introduction of a second 1-hydroxy-2*E*,4*Z*-diene system in AEA led to a complete loss of binding affinity as demonstrated by 5,15-diHAEA and 8,15-diHAEA (Table 1).

AEA also inhibited [³H]CP-55,940 binding to spleen membranes, which express CB₂ receptors, with a K_i of 360 nM (Table 1) in the presence of PMSF. This is in agreement with previous observations.² The CB₂ receptor was more critical in accepting oxygenated metabolites of AEA as ligands than the CB₁ receptor. 12*S*-HAEA and 5*R*-HAEA were almost as potent as AEA (Table 1), while 5*S*-HAEA, 11*S*-HAEA, 15*S*-HAEA, and the doubly hydroxylated AEAs (5,15-diHAEA and 8,15-HAEA) were inactive (Table 1). Interestingly, 13*S*-HLEA had a binding affinity toward the CB₂ receptor with a K_i of 600 nM, whereas it was inactive at the CB₁ receptor.

Interaction with AEA Transporter and FAAH. Human lymphoma U937 cells have a selective AEA transporter with a K_m and V_{max} of 0.13 μM and 140 pmol/min/mg protein, respectively.⁶ These cells also have an active FAAH with a K_m and V_{max} of 6.5 μM and 520 pmol/min/mg protein, respectively.⁶ Introduction of 1-hydroxy-2*E*,4*Z*-diene into AEA at any position disrupted its ability to inhibit the transport of [³H]AEA into U937 cells (Table 2). This indicates that the HAEAs have a reduced binding affinity for the AEA transporter. It has been suggested that at least one *cis* double bond is necessary for binding to the AEA transporter protein and four *cis* double bonds for translocation into the cell.³⁰ Our data are in line with these observations.^{7,30,31}

Table 2. Inhibition Constants (K_i) of AEA and Its Oxygenated Metabolites for FAAH Activity and AEA Transporter Activity

compd	FAAH (μM) ^a	transporter (μM) ^b
AEA	>10	>10
5(S)-HAEA	2.52 ± 0.13	>10
5(R)-HAEA	1.89 ± 0.09	>10
11(S)-HAEA	0.57 ± 0.03	>10
11(R/S)-HAEA	0.69 ± 0.03	>10
12(S)-HAEA	2.90 ± 0.15	>10
13(S)-HLEA	0.43 ± 0.02	>10
15(S)-HAEA	0.63 ± 0.03	>10
15(R/S)-HAEA	0.63 ± 0.03	>10
5,15-diHAEA	1.26 ± 0.06	>10
8,15-diHAEA	0.69 ± 0.03	>10

^a All compounds were competitive inhibitors of FAAH activity in U937 cells. [³H]AEA was used as substrate, in the 0–25 μM concentration range. ^b All compounds were competitive inhibitors of AEA transporter activity in U937 cells. [³H]AEA was used as substrate, in the 0–1000 nM concentration range.

FAAH accepted all AEA derivatives as inhibitors (Table 2), thereby making FAAH the least selective protein of the endocannabinoid system. Introduction of the 1-hydroxy-2*E*,4*Z*-pentadiene system increased the ability of all AEA derivatives to competitively inhibit [³H]AEA hydrolysis by human U937 cells. 13*S*-HLEA was the most potent inhibitor with a K_i of 0.43 μM (23-fold better than AEA), while 12*S*-HAEA had a 3-fold higher K_i than AEA. Introduction of a second hydroxyl group did not improve the inhibition power any further. The rank order was 13*S*-HLEA > 11*S*-HAEA > 15*S*-HAEA ≈ 8,15-diHAEA > 5,15-HAEA > 5*R*-HAEA > 5*S*-HAEA > 12*S*-HAEA. The solubility of HAEAs in aqueous solutions was higher than that of the parent compound, due to the introduction of the hydroxyl function. This improves the feasibility of the use of HAEAs as inhibitors of FAAH, as compared to saturated congeners.

Previously, it was shown that arachidonoyl-based inhibitors were 2–3-fold more potent than oleoyl-based inhibitors. The removal of the oleoyl $\Delta^{9,10}$ *cis* double bond or the incorporation of a trans olefin reduced inhibitor potency.³² The optimal length of the acyl chain appeared to be 8–12 C atoms, which corresponded to the location of the double bond in oleoyl $\Delta^{9,10}$ and in arachidonoyl $\Delta^{8,9/\Delta^{11-12}}$.³² Our results are in good agreement with these findings. Oxygenated AEAs in which C₉ and C₁₂ are sp² C atoms are the most potent inhibitors (13-HLEA, 11*S*-HAEA, 15*S*-HAEA, and 8,15-diHAEA), whereas 12*S*-HAEA (with an sp³ C atom at C₁₂) is the weakest inhibitor. Introduction of a hydroxyl group at C₅ reduces the inhibitor potency of the metabolites.

Interaction of 2-AG and Its Congeners with the Proteins of the Cannabinoid System. 2-AG rapidly isomerizes both *in vitro* and *in vivo*. The rate of this process is increased by high temperature and by acidic or basic pH. Two stereoisomers can be formed, i.e., 1-arachidonoyl-*sn*-glycerol (1-AG) and 3-arachidonoyl-*sn*-glycerol (3-AG) (Figure 1). In endocannabinoid analysis, usually 10–40% of a racemic mixture of 1(3)-AG is found.³³ To date, most interaction studies of 2-AG with proteins of the endocannabinoid system have not accounted for isomerization of 2-AG into 1(3)-AG during the incubation period. Here, it is shown that 2-AG inhibited potently the binding of [³H]CP-55,940 to CB₁ and CB₂ receptors with a K_i of 100 nM (Table 3) in the

Table 3. Inhibition and Displacement Constants (K_i) of 2-AG and Congeners for FAAH Activity, AEA Transporter Activity, and CB₁ and CB₂ Receptor Binding

compd	CB ₁ (nM) ^a	CB ₂ (nM) ^b	FAAH (μ M) ^c	transporter (μ M) ^d
2-AG	100 \pm 20	100 \pm 20	5 \pm 0.25	3 \pm 0.15
1-AG	>1000	>1000	3 \pm 0.15	>10
3-AG	>1000	>1000	2.5 \pm 0.15	10 \pm 0.50
15-HO-1-AG	>1000	550 \pm 80	6 \pm 0.30	9 \pm 0.45
15-HO-3-AG	>1000	>1000	5 \pm 0.25	7 \pm 0.35

^a K_i values were calculated from the displacement curves of [³H]CP-55,940 from rat forebrain membranes in the presence of PMSF. ^b K_i values were calculated from the displacement curves of [³H]CP-55,940 from rat spleen membranes in the presence of PMSF. ^c All compounds were competitive inhibitors of FAAH activity in U937 cells. [³H]AEA was used as substrate, in the 0–25 μ M concentration range. ^d All compounds were competitive inhibitors of AEA transporter activity in U937 cells. [³H]AEA was used as substrate in the 0–1000 nM concentration range.

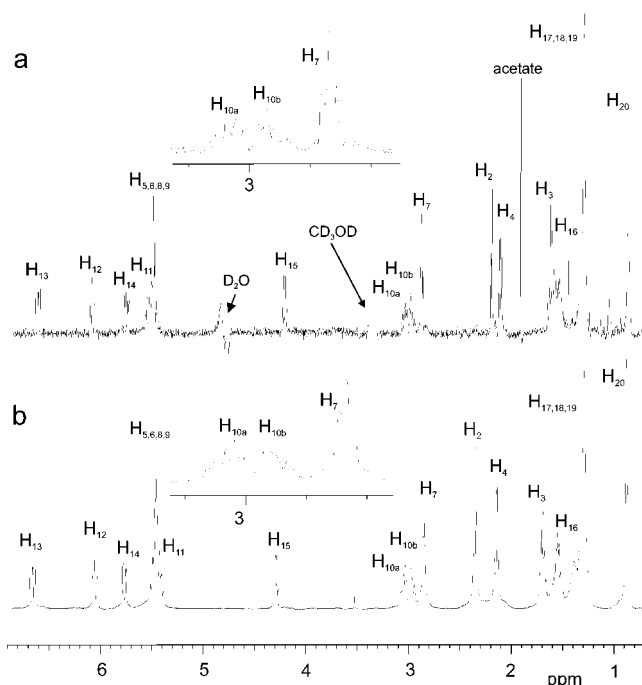
presence of PMSF. 2-AG also inhibited [³H]AEA transport with a K_i of 3 μ M and was 2-fold more potent than AEA in inhibiting FAAH (Table 3). However, 1-AG and 3-AG did not bind to either CB receptor and did not interfere with AEA transport (Table 3). Thus, after it is isomerized, 2-AG is inactivated, thereby decreasing effective concentrations of 2-AG. This uncontrolled isomerization may account to some extent for the large differences in K_i values reported in the literature for 2-AG binding to CB receptors and for its inhibition of AEA transport.⁶

Interestingly, introduction of the 15-hydroxy-11Z,13E-diene system in 1-AG increased its CB₂ binding affinity as compared to its parent compound, but this was not the case for 3-AG. Both 15-HO-1-AG and 15-HO-3-AG could inhibit AEA transport at low micromolar concentrations but were worse inhibitors of [³H]AEA hydrolysis than the parent compounds (Table 3).

It should be noted that different mammalian lipoxygenases are capable of using AEA and 2-AG as substrates in *in vitro* systems.^{27,28,34,35} If this action of lipoxygenases would be functional *in vivo*, this might be instrumental to generate *in vivo* selectivity in the endocannabinoid system. In this line, it has been shown that 5-lipoxygenase inhibitors “disclose” a cryptic FAAH activity in human mast cells.³⁶ Furthermore, the increased capability of HAEAs to inhibit FAAH may be a way to enhance endocannabinoid signaling, *i.e.*, an “entourage” effect for AEA similar to that shown for 2-AG.³⁷

Conformation and Solvation Effects Studied with NMR Spectroscopy. To study the conformational effects induced by different solvents on an acyl chain, one-dimensional (1D) and two-dimensional (2D) NMR spectroscopy experiments were performed with 15(S)-hydroxy-eicosa-5Z,8Z,11Z,13E-tetraenoic acid (15-HETE) in chloroform and water. Double bonds and areas with conjugated double bonds induce considerable conformational restraints to molecules. Therefore, spectral analysis was focused on regions containing signals from these restrained areas and especially on the flexible methyl-ene group regions that connect them.

The NMR spectra of 15-HETE in D₂O and CDCl₃ were remarkably similar in terms of chemical shift values and coupling constants (Figure 2a,b and Supporting Information). The spectral region containing the signals for H₇ and H₁₀, which are regarded as sensitive probes for

**Figure 2.** 1D NMR spectra of 15-HETE in water (a) and chloroform (b).

conformational differences, did not show any notable differences. To get more insight into the conformational properties of 15-HETE, 2D NMR spectra were recorded that reveal information about short interproton distances (nuclear Overhauser enhancement spectroscopy (NOESY) or off-resonance ROESY). In D₂O solutions, the signal-to-noise ratio was poor, despite extended measuring times, due to the low solubility of 15-HETE. Qualitative comparison of NOESY spectra of 15-HETE CDCl₃ solution and off-resonance ROESY spectra in D₂O solution revealed that the more intense cross-peaks were present in both solutions (data not shown). To obtain high quality 2D NMR data of 15-HETE in a polar environment, a NOESY spectrum of 15-HETE was recorded in a CD₃OD solution. This NMR spectrum showed similar spectral properties as had been obtained for CDCl₃ or D₂O solutions, and also, the NOE cross-peaks were qualitatively and quantitatively similar (data not shown). The NOESY spectra did not show any cross-peaks that signify long-range (primary structure) interactions. Thus, analysis of the 1D NMR profiles, chemical shifts, scalar coupling values, and distance correlation spectra did not reveal notable differences, which could originate from different conformations of 15-HETE induced by chloroform, methanol, or water.

Special attention was given to the conjugated pentadiene system. An intense cross-peak in the methanol NOESY spectrum was observed between H₁₂ and H₁₄, whereas the NOE for the interresidual contact between H₁₂ and H₁₃ was less intense (Figure 3a). Proton distances were estimated from cross-peak intensities and were calibrated to distances on the basis of the distance of the vicinal protons H₁₁–H₁₂ (2.20 Å). The distance between H₁₂–H₁₄ was 2.24 Å, and that between H₁₂–H₁₃ was 2.98 Å, which indicated that the dihedral angle C₁₁–C₁₂–C₁₃–C₁₄ was almost exclusively 180° (Figure 3b) rather than 0° (Figure 3c). Thus, a single conformation of the conjugated pentadiene system was indeed strongly preferred.

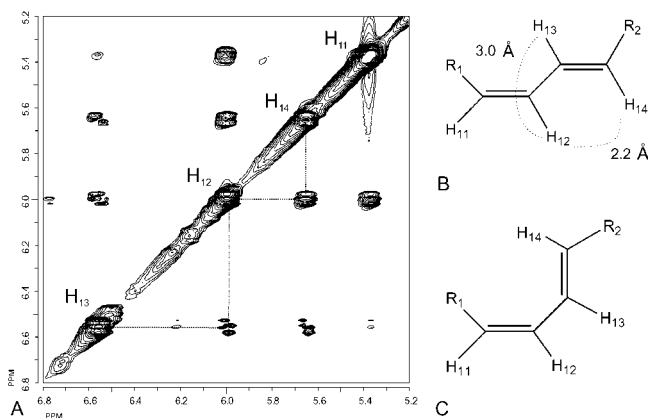


Figure 3. 2D NMR spectrum (NOESY) of 15-HETE (a). The region of interest (6.8–5.2 ppm) is displayed, showing that NOE contacts between H₁₂ and H₁₄ are more intense than H₁₂ and H₁₃. This indicates that the conformation of the conjugated 1-hydroxy-2*Z*,4*E*-pentadiene system is represented by panel b rather than panel c.

Conformational Analysis of (H)AEAs. To develop an endocannabinoid pharmacophore model, an ensemble of active conformations of AEA has to be identified. The conformation of AEA is mainly determined by its acyl chain. The unsaturated acyl chain of AEA is known to adopt many conformations that are energetically almost equivalent and that are not separated by high-energy barriers. This property originates from those areas where two double bonds are separated by one methylene group.³⁸ The conformational space of the two dihedral angles involved shows a large occupied region.³⁹ MD studies were performed with AEA, 5*S*-, 5*R*-, 11*S*-, 12*S*-, and 15*S*-HAEA, to investigate whether the 1-hydroxy-2*E*,4*Z*-pentadiene system was responsible for inducing conformations different from AEA, which affect its ability to adopt folded conformations, and thus its bioactivity.

Previous molecular modeling studies have been performed in vacuo or with solvent treated as a dielectric continuum.^{23–25,40} It has been shown that the choice of the solvent influenced the shape of AEA, which was basically extended in chloroform or in vacuo, while it was more compact in water.⁴⁰ It has been suggested that a compact shape reduces the exposure of hydrophobic portions.²⁰ However, our NMR data indicate that the choice of solvent does not notably influence the average conformation of the acyl chain of 15-HETE. We have performed MD simulations with explicit water molecules instead of chloroform to mimic physiological conditions.

Analysis of all dihedral angles of the MD trajectories of AEA and the HAEA compounds showed a number of common features. The dihedral angle of bonds between two methylene groups was predominantly 180°, but also, many short visits to –60 and 60° were observed. The dihedral angle of bonds between a hydroxymethylene carbon and an sp² carbon of a conjugated double bond was chiefly –140° but showed a number of transitions to 60°. The dihedral angle of bonds between a hydroxymethylene carbon and an sp² carbon of a (nonconjugated) double bond was mainly 170° but visited 60° many times. The dihedral angles of bonds inside a 1*Z*,4*Z*-pentadiene system involving a methylene group and an sp² carbon could be any of –60, –120, 180, 120,

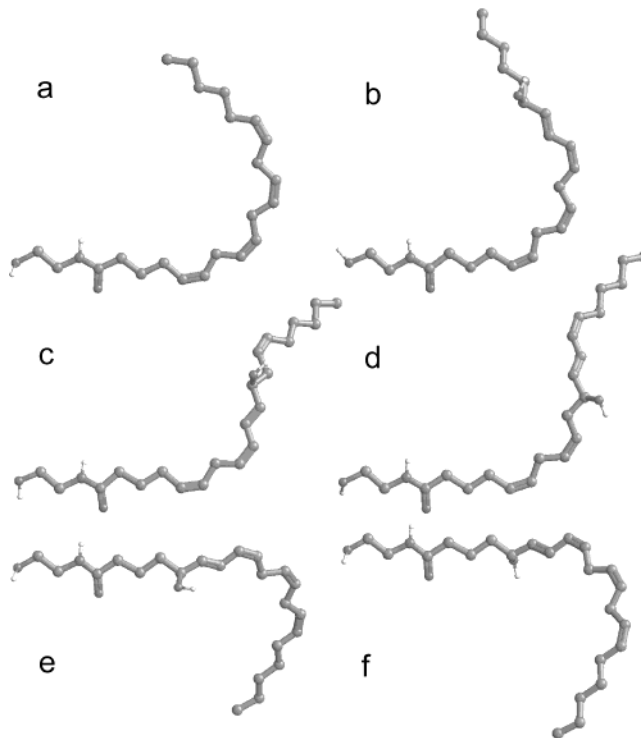


Figure 4. Idealized conformations of compounds (a) AEA, (b) 15*S*-HAEA, (c) 12*S*-HAEA, (d) 11*S*-HAEA, (e) 5*R*-HAEA, and (f) 5*S*-HAEA. The dihedral angles for the free rotational bonds in the 1*Z*,4*Z*-pentadiene systems could take any value from 60° going via 180 to –60° and were set to 180°.

60° and all values between, with some preference for –120 and 120°. The many transitions observed for all of these dihedral angles indicate low-energy barriers and facilitate adequate sampling of the conformational space.

Idealized conformations of AEA and HAEAs are displayed in Figure 4, with all dihedral angles set to the most populated orientations according to the MD trajectories. It is shown that the 1*Z*,4*Z*-pentadiene systems induce bent-shaped conformations. When both dihedral angles for the free rotational bonds in the 1*Z*,4*Z*-pentadiene systems, denoted φ_1 and φ_2 , are set to 180°, a bent shape for AEA is observed. In addition, when φ_1 , φ_2 have opposite signs, e.g., 120, –120°, again a bent shape emerges. Only, when both dihedrals have the same signs, the shape of the molecule is more stretched. As opposite signs and equal signs occur with equal abundance and dihedral angles around 180° also result in bent shapes, more than half of the low-energy conformations have shapes that are bent. This is in contrast to saturated acyl chains, where a dihedral angle of 180° is favored leading to an extended shape. This makes strongly bent shapes energetically unfavorable for saturated aliphatic chains (see also Rich³⁹). Therefore, it seems that the easy adaptation of folded conformations of polyunsaturated acyl chains originates in the inclination of 1*Z*,4*Z*-pentadiene systems to form bent shapes and is not so much a result of the flexibility of the chains as previously suggested.²⁰

Introduction of a conjugated double bond in AEA, by creating a 1-hydroxy-2*E*,4*Z*-pentadiene system, transfers a nonrotatable bond with a dihedral angle of 0° to a new nonrotatable bond with a dihedral angle of 180° (1*Z* to 2*E*). Therefore, it changes the global shape of the

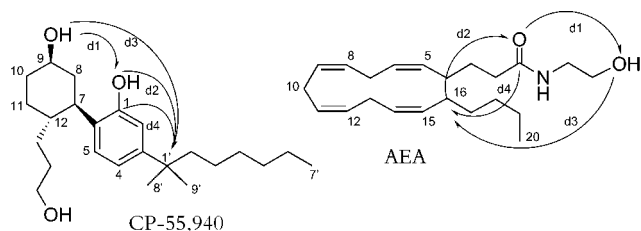


Figure 5. Distances and numbering of CP-55,940 and AEA.

chain. It also makes the chain rigid as it essentially fixates the middle bond in the conjugated system to 180° , which results in six carbon atoms lying in one plane. Conjugation of the pentadiene system (such as depicted in the specific conformation of AEA in Figure 4a) results in more extended chains for 12*S*-HAEA (Figure 4c) and 11*S*-HAEA (Figure 4d), while in 5*R*-HAEA (Figure 4e) and 5*S*-HAEA (Figure 4f) the chains are not more extended but the direction of the loops is influenced.

Structural Comparison of Pharmacophores of (H)AEAs with CP-55,940. To investigate whether the introduction of the 1-hydroxy-2*E*,4*Z*-pentadiene system in AEA influenced the orientation and distances of pharmacophoric groups in the HAEAs, the pharmacophores of the reference compound CP-55,940 were compared with pharmacophores in the (H)AEA series (Figure 5). The pharmacophoric groups were identified based on the model of Tong et al.²⁵ This model was capable of discriminating between structurally related compounds exhibiting different pharmacological potencies for the CB₁ receptor, i.e., AEA and prostaglandinethanolamide. Furthermore, it could be used in a three-dimensional quantitative structure–activity relationship (3D QSAR) study to predict the K_i value of AEA. The following pharmacophoric units in CP-55,940, (i) the phenolic hydroxyl oxygen, (ii) the cyclohexyl hydroxyl oxygen, and (iii) the first carbon on the alkyl side chain (C_1'), closely match to (i) the oxygen of the carbonyl, (ii) the hydroxyl oxygen, and (iii) the first carbon of the pentyl tail (C_{16}) in the (H)AEA series. In the model of Tong et al., the pyran oxygen of THC (or HHC) was not included as pharmacophoric unit, as was done in the model of Thomas et al.,²³ since it is not considered essential for the interaction. The model of Tong was chosen because in our studies synthetic [³H]-CP-55,940 (Figure 1), which also lacks the pyran oxygen, was used to determine displacement constants of HAEAs at both CB₁ and CB₂ receptors. Furthermore, the cyclohexyl OH in the cannabinoids and the corresponding terminal OH of AEA both enhance binding, but their absence (as in THC and alkyl arachidonate derivatives) does not eliminate activity.²⁵

First, the conformation of CP-55,940 was analyzed to find the orientation of the hexyl ring in relation to the phenyl ring, and the orientation of the alkyl side chain. NOESY data for CP-47,497 (in chloroform) have shown that the orientation of the two rings around the C_6 – C_7 bond, determined by the dihedral angle C_5 – C_6 – C_7 – C_8 (see Figure 5 for numbering), is -60° rather than 120° .⁴¹ In this orientation, the OH of the cyclohexyl ring is at the same side of the phenolic ring, as is the case for HHC–DMH. This is in agreement with the proposal that the dihedral angle $O_{\text{hexyl}}-C_9-C_1-O_{\text{phenyl}}$ (which is -90° for CP-55,940) must be negative, to get the most

active conformation.⁴² The NMR data⁴¹ have also indicated that the 1',1'-dimethylheptyl side chain can occur in four different orientations in relation to the phenyl ring, with almost equal probability. To get the positions of the pharmacophores, a MD simulation of CP-55,940 was performed with the orientation of the rings following that of CP-47,497.

The CP-55,940 acyl chain has no single preferred orientation, and it is not yet known how it is oriented when it binds to the receptor. This hampers an easy comparison with the orientation of the tail of the acyl chain of the (H)AEA series. To facilitate the comparison of the orientation of the pentyl chain between different compounds, the orientation of the pentyl chain was expressed in polar coordinates, by using the orientation of vector $C_{1'}-C_{2'}$ relative to the $O_{\text{phenyl}}-C_1-C_{1'}$ plane for CP-55,940 and $C_{16}-C_{17}$ relative to the $O_{\text{carbonyl}}-C_1-C_{16}$ plane for the (H)AEA series. (For CP-55,940, φ = dihedral angle $O_{\text{phenyl}}-C_1-C_{1'}-C_{2'}$ and θ = angle $C_1-C_{1'}-C_{2'}$, and for the (H)AEA series, φ = dihedral angle $O_{\text{carbonyl}}-C_1-C_{16}-C_{17}$ and θ = angle $C_1-C_{16}-C_{17}$.)

The following four atoms were used to analyze the atom positions of the pharmacophores: phenolic oxygen, cyclohexyl oxygen, C_1 and $C_{1'}$ for CP-55,940, and the carboxyl oxygen, the oxygen of the ethanol, C_1 and C_{16} for the (H)AEAs, respectively. Average distances between the pharmacophores in CP-55,940 are as follows: phenolic and cyclohexyl oxygen = 0.63 nm (**d1**), cyclohexyl oxygen and $C_{1'}$ = 0.91 nm (**d3**), phenolic oxygen and $C_{1'}$ = 0.49 nm (**d2**). The distance between the oxygen of the carboxyl and the oxygen of the ethanol in the (H)AEA series (**d2**) is somewhat smaller (0.55 nm). The distances **d2** and **d3** in the (H)AEA series demonstrate a large degree of variation, as shown in Figure 6. In the same figure, the region of distances in CP-55,940 is indicated by an ellipse that is marked by an arrow. This CP-55,940 region falls within the much broader region of the (H)AEA series for all members, except for 5*R*-HAEA.

From the MD simulations of the (H)AEA series, all frames were selected that had appropriate $O_{\text{hydroxyl}}-C_{16}$ (**d3**), $O_{\text{carbonyl}}-C_{16}$ (**d2**), and C_1-C_{16} (**d4**) distances (Figure 7) and from these frames, the orientation of vector $C_{16}-C_{17}$ was determined. The results of the CP-55,940 run are indicated in Figure 7 by the region between the curved lines. The MD simulations of 11*S*-HAEA and 5*R*-HAEA did contain only a few frames with matching distances. As 5*R*-HAEA and 5*S*-HAEA are enantiomers, the MD runs of these compounds must furnish the same results in distances after adequate conformational sampling. This is clearly not the case after 5 ns. MD simulations show the presence of the required conformations in most of the simulations; therefore, it can be concluded that the required conformations have sufficiently low energy to make their existence feasible. The results of the simulations of AEA and 12*S*-HAEA display a great similarity. For both simulations, many conformations emerge inside the CP-55,940 region enclosed by $60^\circ > \varphi > 180^\circ$. This region is scarcely populated for 5*R*-HAEA and 5*S*-HAEA, and not at all for 15*S*-HAEA and 11*S*-HAEA. It is tempting to suggest a preference for analogous orientations of the pentyl tail for AEA and 12*S*-HAEA, which have a similar affinity for the CB₁ receptor, while the low

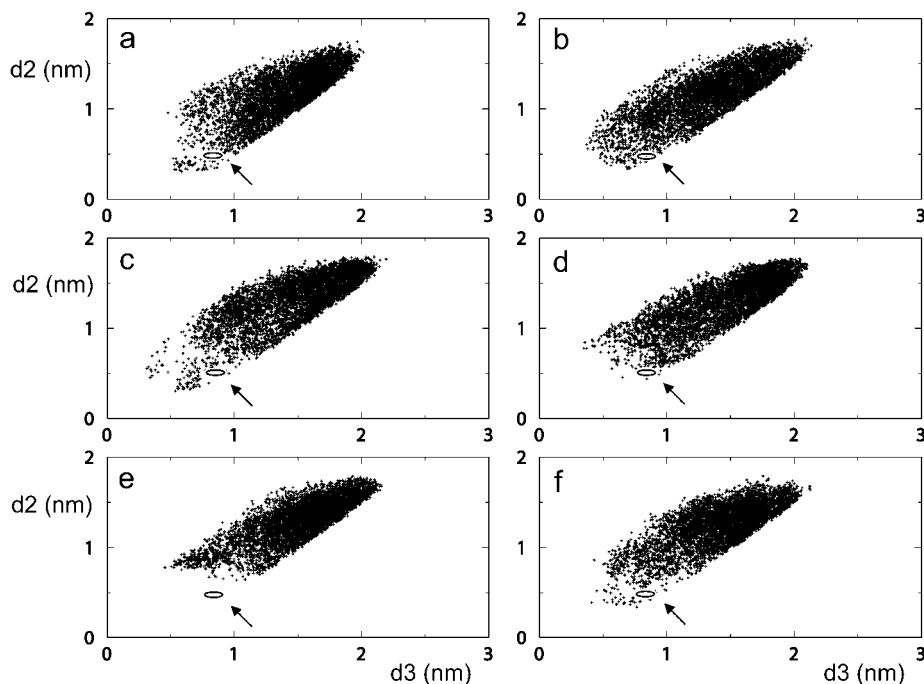


Figure 6. Scatter plots of distances **d3** and **d2** obtained during simulation of compounds (a) AEA, (b) 15*S*-HAEA, (c) 12*S*-HAEA, (d) 11*S*-HAEA, (e) 5*R*-HAEA, and (f) 5*S*-HAEA. The corresponding region of CP-55,940 is inside the ellipse and indicated by the arrow. Frames were selected with a time step of 1 ps.

affinity and inactive ligands do not show a preference for this pentyl tail orientation.

Structural Alignment of CP-55,940 and Restrained (H)AEAs. The MD simulations of the (H)AEA series do not provide enough suitable configurations for analysis; therefore, the positions of the pharmacophores in the (H)AEA series were aligned with those of the pharmacophores in CP-55,940. For that purpose, MD simulations were performed with positionally restrained atoms representing the pharmacophores according to the model of Tong et al.²⁵ Stereospecificity is important, as indicated by differences in activity of the enantiomers 5*R*-HAEA and 5*S*-HAEA. To take this stereospecificity into account, a minimum of four atom positions has to be restrained. Selected atoms were the oxygen in the ethanol hydroxyl, the C₁₆ atom of the aliphatic chain, and the carbon and oxygen in the carboxyl. Both carboxyl carbon and oxygen positions were chosen, to make sure that the availability of the oxygen for binding to CB₁ is not diminished by possible shielding by the position of the carbon. The results of the MD simulations for the orientation of the pentyl tail for AEA and all HAEAs are given in Figure 8. As expected, this orientation (represented by the vector C₁₆–C₁₇) in the (H)AEA series is less restricted than that of the corresponding vector C₁–C₂ in the acyl chain of CP-55,940. However, the overlapping regions of CP-55,940 and the (H)AEA series do not reveal great differences between the various (H)AEAs investigated. The differences in binding cannot be explained by these results.

The most populated overlapping region of CP-55,940 and AEA in Figure 8 was with $\varphi \approx 50^\circ$ and $\theta \approx 100^\circ$. An illustrative configuration is selected from that region and is presented in Figure 9. It demonstrates the flexible hairpin-shaped loop C₂ to C₁₅ of AEA that does not correspond to any part of CP-55,940 and that accommodates the differences in the various (H)AEA

compounds. Configurations from the restrained MD simulations of the (H)AEA compounds with a C₁₆–C₁₇ vector orientation of $\varphi, \theta = 50, 100^\circ$ were selected and studied for differences in the orientation and shape of this loop.

It turns out that restrained MD simulations yield conformations of the (H)AEAs that are very much the same, as demonstrated by 11*S*-HAEA and 12*S*-HAEA. This becomes evident from the orientation of the C₁₆–C₁₇ vector in Figures 8 and 10. The shape of the C₂ to C₁₅ loop differs slightly in the various HAEAs, due to the different positions of the hydroxyl and conjugated double bonds that define a “six atoms in a plane” stiff part. Note that the loop formed by the carbons C₂ to C₁₅ adopted various conformations during the simulations. Nevertheless, the conformational space of the orientation of the loop C₂ to C₁₅, relative to the orientation of the C₁₆–C₁₇ tail vector, is essentially identical for both compounds during the simulations (data not shown).

Conclusions

Toward the Design of Selective Molecular Probes for Interaction with the Proteins of the Cannabinoid System. This study has shown that restricting the flexibility of AEA and 2-AG and introducing hydroxyl functions in their acyl chains brings selectivity and attenuates their binding potency toward the proteins of the endocannabinoid system. Although the displacement constants were modest, 15*S*-HAEA selectively bound to the CB₁ receptor, whereas 13*S*-HLEA and 15-HO-1-AG were the only eicosanoid ligands that selectively bound to the CB₂ receptor to date. 11*S*-HAEA did not bind to CB₁ or CB₂ receptors but was a very good inhibitor of FAAH ($K_i = 0.57 \mu\text{M}$). By contrast, 12*S*-HAEA bound both CB receptors with an affinity similar to that of AEA, but it was a poor inhibitor of FAAH.

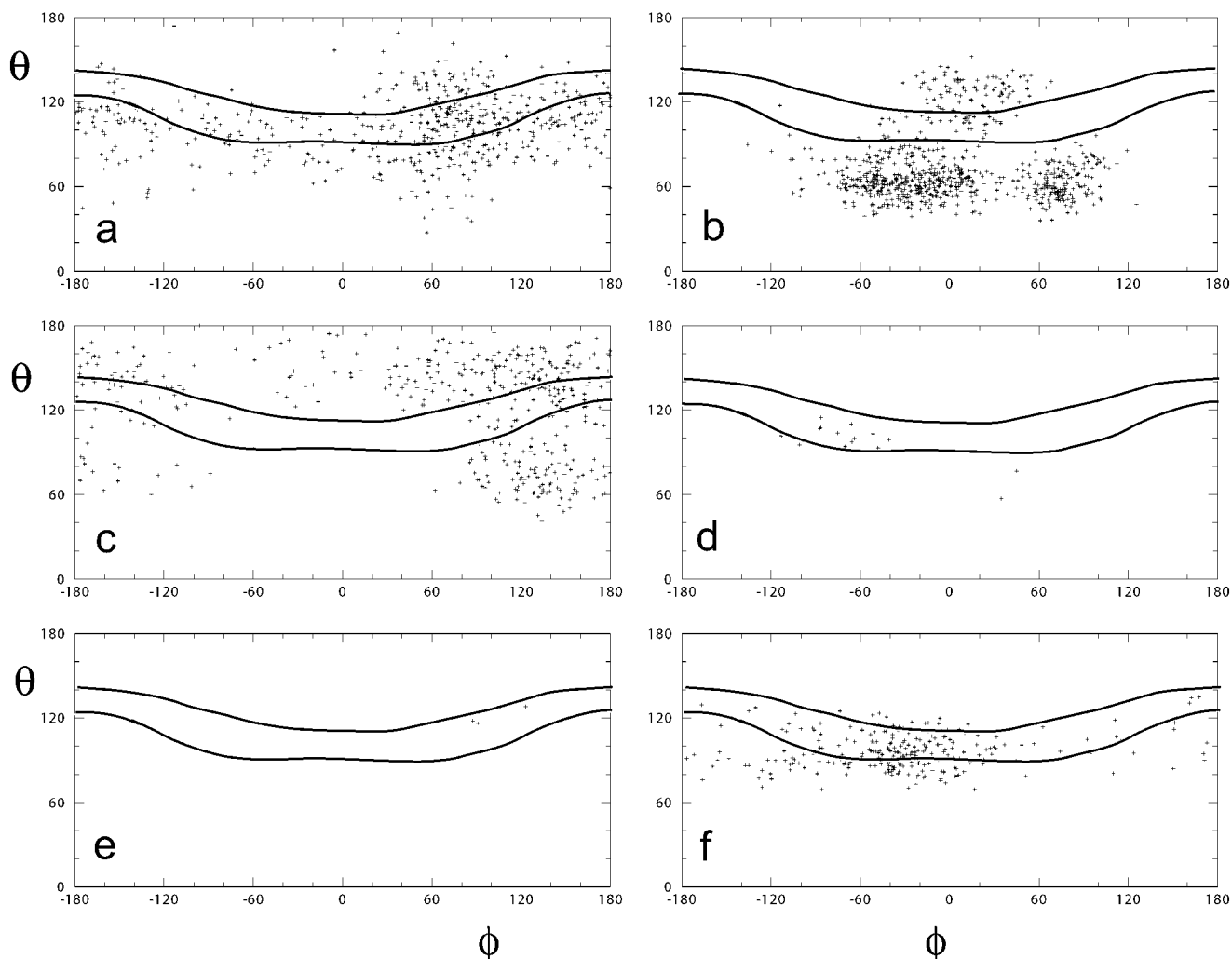


Figure 7. Scatter plots of the orientation of vector $C_{16}-C_{17}$, expressed in polar coordinates, during the 5 ns MD simulation of compounds (a) AEA, (b) 15*S*-HAEA, (c) 12*S*-HAEA, (d) 11*S*-HAEA, (e) 5*R*-HAEA, and (f) 5*S*-HAEA, for frames that had distances $d_2 < 0.55$ nm, $d_3 < 0.95$ nm, and $d_4 < 0.55$ nm. Frames were selected with a time step of 0.1 ps. The corresponding results of the CP-55,940 simulation are indicated by the region between the curved lines. For CP-55,940, φ = dihedral angle $O_{\text{phenyl}}-C_1-C_1-C_2'$ and θ = angle $C_1-C_1-C_2'$, and for the (H)AEAs, φ = dihedral angle $O_{\text{carbonyl}}-C_1-C_{16}-C_{17}$ and θ = angle $C_1-C_{16}-C_{17}$.

Nevertheless, all HAEAs displayed an increased potency to inhibit FAAH, whereas their ability to interact with the AEA transporter was disrupted ($K_i > 10 \mu\text{M}$). This makes it possible to discern the physiological contribution of FAAH and AEA transporter in the clearance of endocannabinoids. Thus, the HAEAs can serve as structural templates to generate selectivity in the endocannabinoid system and may possibly be used as targets for drug development.

The NMR experiments indicated that chloroform and water did not induce different conformations in the acyl chain of 15-HETE. Consequently, there were no indications that 15-HETE would adopt a more compact overall conformation in aqueous solutions. For the first time, MD simulations of AEA and derivatives were performed that included explicit water molecules. Conformation analysis revealed that polyunsaturated fatty acids such as AEA assume more folded conformations than saturated fatty acids, because of an inclination of the 1*Z*,4*Z*-pentadiene subsystems to form bent shapes. Furthermore, our data indicated that the ability to adopt a tightly folded conformation is not the only essential feature of the acyl chain, which enables AEA to bind to the CB₁ receptor. In the free MD simulations, all HAEA

derivatives, both active and inactive at the CB₁ and CB₂ receptors, could adopt a folded conformation in which the pharmacophores in AEA closely matched those of CP-55,940. Close inspection of the free and restrained MD simulations of the HAEA series indicated that the differences must be located in the conformational details of the loop (C_2 to C_{15}), e.g., the position and orientation of the hydroxyl group. Furthermore, evaluation of the binding data indicated that an sp^2 carbon is required at position C_{11} in AEA derivatives for binding to the CB₁ receptor. The free MD simulations may suggest that the pentyl tail orientations of the high-affinity ligands AEA and 12*S*-HAEA are different from those of the low-affinity and inactive ligands. Distinct differences in terms of tail and loop orientations between high-affinity CB₁ receptor ligands and inactive compounds could not be detected in the restrained MD simulation. Our data also indicated that the binding of HAEAs to the CB₂ receptor is more sensitive toward steric hindrance along the acyl chain. However, more conclusive statements about the nature of the interactions of the CB receptors with their ligands await purification and crystallization of the proteins with their ligands.

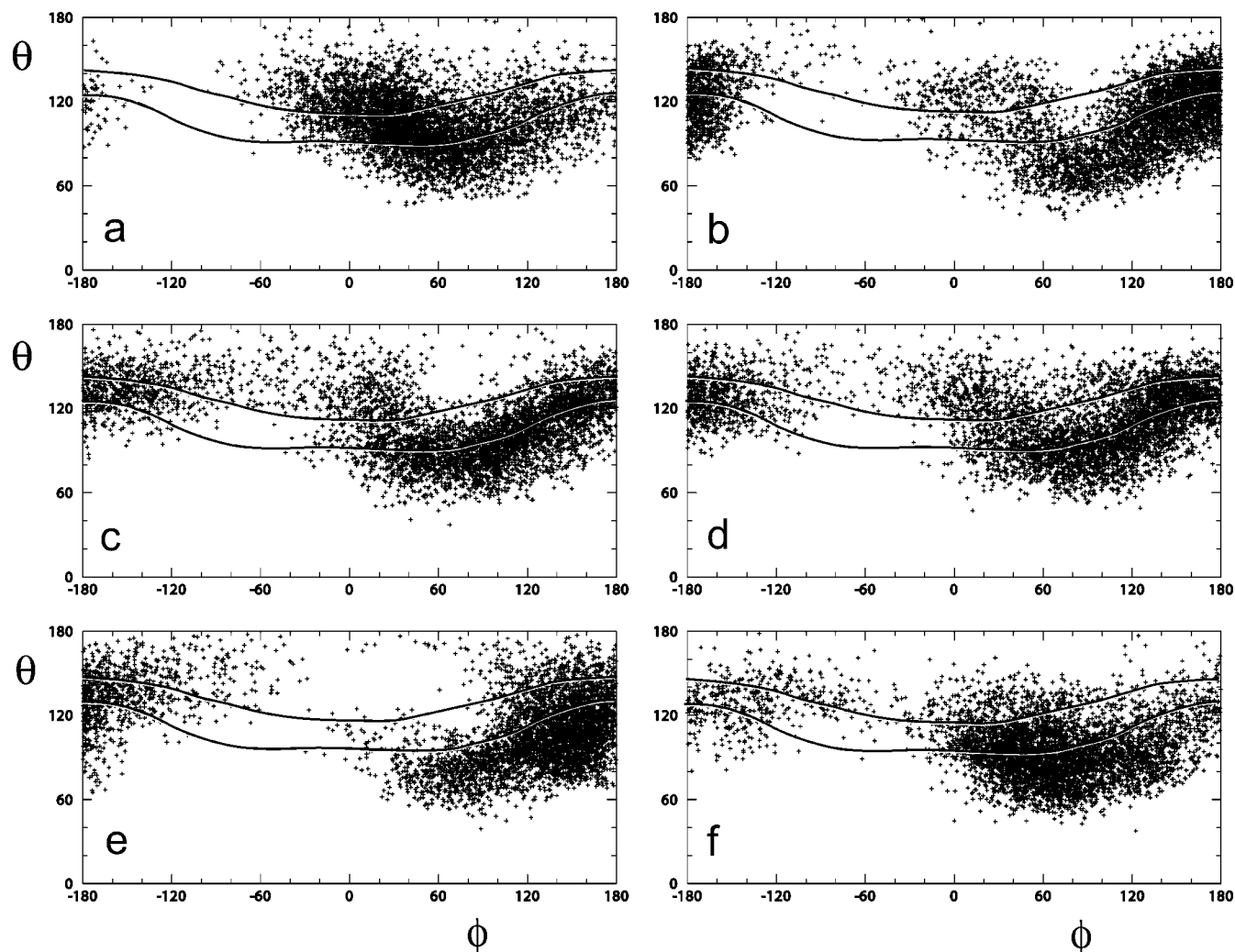


Figure 8. Scatter plots of the orientation of vector $C_{16}-C_{17}$, expressed in polar coordinates, during the 5 ns restrained MD simulation of compounds (a) AEA, (b) 15*S*-HAEA, (c) 12*S*-HAEA, (d) 11*S*-HAEA, (e) 5*R*-HAEA, and (f) 5*S*-HAEA. Frames were selected with a time step of 1 ps. The corresponding results of the CP-55,940 simulation are indicated by the region between the curved lines.

Materials and Methods

Synthesis of 1(3)-Arachidonoyl-*sn*-glycerol. Arachidonic acid (1 equiv) was activated by 20 equiv of oxalyl chloride in dry dichloromethane. The mixture was stirred for 2 h under nitrogen on ice. Excess oxalyl chloride and dichloromethane were evaporated under a nitrogen stream. Arachidonoyl chloride was dissolved in dry dichloromethane/pyridine (1:1), and 10 equiv of (*S*)- or (*R*)-2,2-dimethyl-1,3-dioxolane-4-metanol (1,2- or 2,3-isopropylidene-*sn*-glycerol, respectively) (Fluka Chemical) was added with a catalytic amount of (dimethylamino)pyridine. The reaction was stirred for 12 h under nitrogen on ice and stopped by evaporation of the solvent by a nitrogen stream. The product was dissolved in dichloromethane/acetone (95/5) and purified on SiO_2 ($R_f = 0.72$). A colorless oil was obtained in a yield of 60%. Isopropylidene-1(3)-arachidonoyl-*sn*-glycerol was stored at $-20^\circ C$ until use. Deprotection was carried out as described.⁴³

Biosynthesis of Oxygenated Endocannabinoids. 5-HAEA, 11*S*-HAEA, 15-HAEA, 13*S*-LEA, 5,15-diHAEA, 8,15-diHAEA, 15*S*-HAEA, 15-HO-3-AG, and 15-HO-1-AG were enzymatically synthesized by soybean and barley lipoxygenases (specific activity: 40 and 55 U (μmol linoleic acid min^{-1}) mg^{-1} , respectively) as previously reported and characterized by circular dichroism (CD) spectroscopy, ^1H NMR, and gas chromatography/mass spectrometry (GC/MS).^{28,44-48} The spectra were in accordance with their chemical structures, as previously reported.^{28,44,47,48} Each lipoxygenase was incubated with LEA, AEA (Cayman Chemicals), 3-AG, or 1-AG (1 U

enzyme lipoxygenase per 3 μmol substrate) in 100 mM sodium borate buffer (pH 9 for soybean and pH 7 for barley grain). AEA was incubated with bovine polymorphonuclear leukocytes in phosphate-buffered saline (pH 7.4) to produce 12*S*-HAEA. The products of the plant lipoxygenases were reduced by 3 equiv of sodium borohydride. The HAEAs were isolated with SPE (Bakerbond, 500 mg), analyzed, and purified by reversed phase and chiral phase high-performance liquid chromatography (HPLC) as reported.^{44,45,48} [^3H]AEA (223 Ci/mmol) and [^3H]CP-55,940 (126 Ci/mmol) were purchased from NEN Life Science Products, Inc.

5*R/S*-HAEA. [5(*R/S*)-Hydroxy-eicosa-6*E*,8*Z*,11*Z*,14*Z*-tetraenoyl-*N*-(2-hydroxyethyl)amine]. Barley lipoxygenase: ^1H NMR (CDCl_3): δ 6.55 (dd, $J = 13.6, 10.6$ Hz 1H), 6.02 (t, $J = 10.5$ Hz 1H), 5.71 (dd, $J = 13.6$ Hz, 1H), 5.39 (m, 5H), 4.16 (m, 1H), 3.72 (t, 2H), 3.42 (q, 2H), 2.97 (m, 2H), 2.81 (m, 2H), 2.22 (t, $J = 7.8$ Hz, 2H), 2.11 (m, 2H), 1.72 (q, $J = 6.2$ Hz 2H), 1.34 (m, 6H), 0.89 (t, $J = 6.2$ Hz, 3H). NaBH_4 and H_2 reduced trimethyl silyl ether GC/MS m/z 515 [M^+], 500 [$\text{M}^+ - \text{CH}_3$], 313 [$\text{C}_{16}\text{H}_{32}\text{OTMS}^+$], 304 [$\text{M}^+ - \text{C}_{15}\text{H}_{31}$], 214 [304-TMSOH], 116 [$\text{C}_2\text{H}_3\text{OTMS}^+$], 73 [TMS^+].

11*S*-HAEA. [11(*S*)-Hydroxy-eicosa-5*Z*,8*Z*,12*E*,14*Z*-tetraenoyl-*N*-(2-hydroxyethyl)amine]. Barley lipoxygenase: ^1H NMR (CDCl_3): δ 6.52 (dd, $J = 11.0; 10.1$ Hz 1H), 5.98 (t, $J = 11.0$ Hz 1H), 5.69 (dd, $J = 15.1; 6.5$ Hz 1H), 5.40 (m, 5H), 4.23 (q, 2H), 3.72 (t, $J = 4.6$ Hz, 2H), 3.42 (q, $J = 5.5$ Hz; 2H), 2.81 (m, 2H), 2.32 (m, 2H), 2.22 (t, $J = 7.4$ Hz; 2H), 2.12 (m, 4H), 1.73 (q, 2H), 1.25-1.38 (m, 6H), 0.88 (t, $J = 6.9$ Hz 3H).

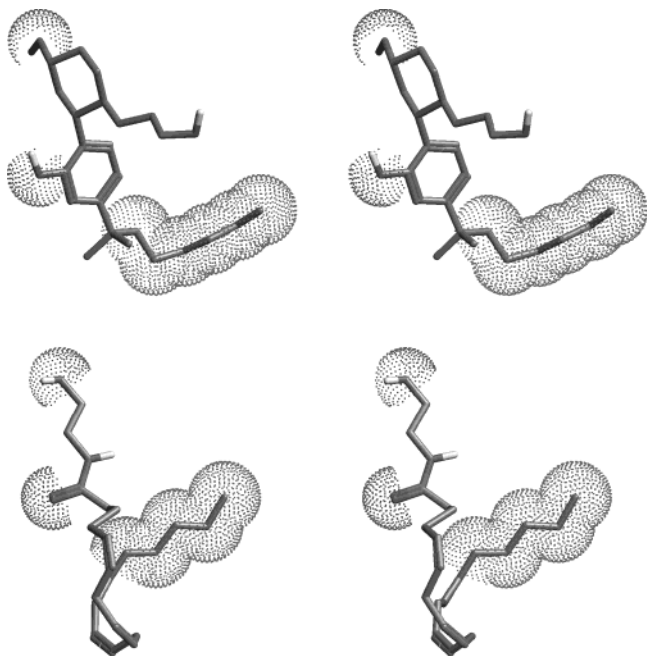


Figure 9. Stereoview of snapshots CP-55,940 (upper panel) and AEA (lower panel) with a vector $C_{16}-C_{17}$ orientation of φ , $\theta = 50, 100^\circ$, depicted with dotted van der Waals surfaces of the pharmacophores to highlight corresponding positions.

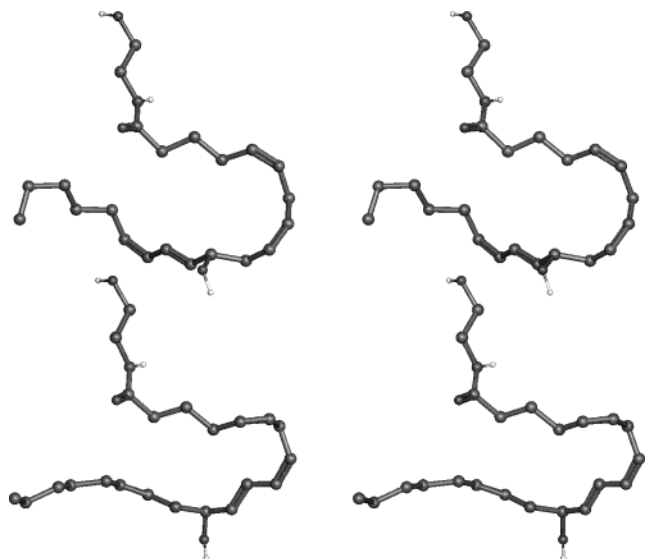


Figure 10. Stereoview of snapshots of 12S-HAEA (upper panel) and 11S-HAEA (lower panel) with vector $C_{16}-C_{17}$ orientation of φ , $\theta = 56, 105^\circ$.

NaBH_4 and H_2 reduced trimethyl silyl ether GC/MS m/z 515 [M^+], 500 [M^+-CH_3], 388 [$\text{M}^+-\text{C}_9\text{H}_{19}$], 229 [$\text{C}_{10}\text{H}_{20}\text{OTMS}^+$], 116 [$\text{C}_2\text{H}_3\text{OTMS}^+$], 73 [TMS^+].

12S-HAEA. [12(S)-Hydroxy-eicosa-5Z,8Z,10E,14Z-tetraenoyl-N-(2-hydroxyethyl)amine]. Bovine leukocytes: $^1\text{H NMR}$ (CDCl_3): δ 6.58 (dd, $J = 14.2$ Hz 1H), 5.99 (t, $J = 10.5$ Hz 1H), 5.74 (dd, $J = 6.2$ Hz 1H), 5.40 (m, 5H), 4.25 (q, 1H), 3.72 (t, $J = 4.6$ Hz 2H), 3.42 (q, $J = 4.6$ Hz 2H), 2.95 (m, 2H), 2.33 (m, 2H), 2.21 (t, $J = 7.5$ Hz 2H), 2.10 (m, 4H), 1.74 (q, $J = 7.3$ Hz, 2H), 1.28 (m, 6H), 0.89 (t, $J = 6.9$ Hz 3H). NaBH_4 and H_2 reduced trimethyl silyl ether GC/MS m/z 515 [M^+], 500 [M^+-CH_3], 402 [$\text{M}^+-\text{C}_8\text{H}_{17}$], 215 [$\text{C}_9\text{H}_{18}\text{OTMS}^+$], 116 [$\text{C}_2\text{H}_3\text{OTMS}^+$], 73 [TMS^+].

15S-HAEA. [15(S)-Hydroxy-eicosa-5Z,8Z,11Z,13E-tetraenoyl-N-(2-hydroxyethyl)amine]. Soybean lipoxygenase: $^1\text{H NMR}$ (CDCl_3): δ 6.55 (dd, $J = 15.4; 12.2$ Hz 1H), 6.00 (t, $J = 10.7$ Hz, 1H), 5.72 (dd, $J = 7.2$ Hz, 1H), 5.40 (m, 5H),

4.12 (q, 1H), 3.72 (t, 2H) 3.42 (q, 2H), 2.97 (m, 2H), 2.82 (m, 2H), 2.22 (t, $J = 7.5$ Hz, 2H), 2.11 (m, 2H), 1.72 (q, $J = 7.3$ Hz, 2H), 1.56 (m, 2H), 1.31 (m, 6H), 0.89 (t, $J = 6.9$ Hz, 3H). NaBH_4 and H_2 reduced trimethyl silyl ether GC/MS m/z 515 [M^+], 500 [M^+-CH_3], 444 [$\text{M}^+-\text{C}_5\text{H}_{11}$], 173 [$\text{C}_6\text{H}_{11}\text{OTMS}^+$], 116 [$\text{C}_2\text{H}_3\text{OTMS}^+$], 73 [TMS^+].

5,15-diHAEA. [5,15-Dihydroxy-eicosa-6E,8Z,11Z,13E-tetraenoyl-N-(2-hydroxyethyl)amine]. Soybean lipoxygenase: $^1\text{H NMR}$ (CDCl_3): δ 6.58 (m, 2H), 6.01 (m, 2H), 5.72 (m, 2H), 5.43 (m, 2H), 4.21 (m, 2H), 3.72 (t, $J = 4.6$ Hz, 2H), 3.42 (q, $J = 4.6$ Hz, 2H), 2.97 (m, 2H), 2.28 (t, $J = 6.9$ Hz, 2H), 1.76 (m, 2H), 1.57 (m, 4H), 1.30 (m, 6H), 0.89 (t, 3H). NaBH_4 and H_2 reduced trimethyl silyl ether GC/MS m/z 603 [M^+], 588 [M^+-CH_3], 532 [$\text{M}^+-\text{C}_5\text{H}_{11}$], 304 [$\text{M}^+-\text{C}_{15}\text{H}_{31}$], 214 [304-TMSOH], 116 [$\text{C}_2\text{H}_3\text{OTMS}^+$], 73 [TMS^+].

8,15-diHAEA. [8,15-Dihydroxy-eicosa-5Z,9E,11Z,13E-tetraenoyl-N-(2-hydroxyethyl)amine]. Soybean lipoxygenase: $^1\text{H NMR}$ (CDCl_3): δ 6.70 (m, 2H), 5.97 (m, 2H), 5.74 (m, 2H), 5.46 (m, 2H), 4.27 (m, 1H), 4.18 (m, 1H), 3.72 (t, $J = 4.6$ Hz, 2H), 3.42 (q, $J = 4.6$ Hz, 2H), 2.32 (m, 2H), 2.19 (t, $J = 6.9$ Hz, 2H), 2.09 (q, 2H), 1.70 (m, 2H), 1.50 (m, 2H), 1.32 (m, 6H), 0.88 (t, 3H). NaBH_4 and H_2 reduced trimethyl silyl ether GC/MS m/z 603 [M^+], 588 [M^+-CH_3], 532 [$\text{M}^+-\text{C}_5\text{H}_{11}$], 346 [$\text{M}^+-\text{C}_{12}\text{H}_{24}\text{OTMS}$], 173 [$\text{C}_6\text{H}_{11}\text{OTMS}^+$], 116 [$\text{C}_2\text{H}_3\text{OTMS}^+$], 73 [TMS^+].

13S-HLEA. [13(S)-Hydroxy-octadeca-9Z,11E-dienoyl-N-(2-hydroxyethyl)amine]. $^1\text{H NMR}$ (CDCl_3): δ 6.49 (dd, $J = 15.0, 11$ Hz, 1H), 5.98 (t, $J = 10.9$ Hz, 1H), 5.67 (dd, $J = 15.2, 6.8$ Hz, 1H), 4.16 (q, $J = 6.5$ Hz, 1H), 3.72 (t, 2H), 3.42 (q, 2H), 2.17 (m, $J = 7.4$ Hz, 4H), 1.66–1.47 (m, 6H), 1.38–1.22 (m, 10H), 0.89 (t, $J = 6.5$ Hz, 3H). NaBH_4 and H_2 reduced trimethyl silyl ether GC/MS m/z 487 [M^+], 472 [M^+-CH_3], 416 [$\text{M}^+-\text{C}_5\text{H}_{11}$], 173 [$\text{C}_6\text{H}_{11}\text{OTMS}^+$], 116 [$\text{C}_2\text{H}_3\text{OTMS}^+$], 73 [TMS^+].

1-AG. $^1\text{H NMR}$ (CDCl_3): δ 5.40 (m, 8H), 4.19 (m, 2H), 3.93 (m, 1H), 3.65 (m, 2H), 2.84 (m, 6H), 2.37 (t, $J = 7.5$ Hz, 2H), 2.09 (m, 4H), 1.72 (m, 2H), 1.33 (m, 6H), 0.89 (t, $J = 6.8$ Hz, 3H).

3-AG. $^1\text{H NMR}$ (CDCl_3): δ 5.40 (m, 8H), 4.19 (m, 2H), 3.93 (m, 1H), 3.65 (m, 2H), 2.84 (m, 6H), 2.37 (t, $J = 7.5$ Hz, 2H), 2.09 (m, 4H), 1.72 (m, 2H), 1.33 (m, 6H), 0.89 (t, $J = 6.8$ Hz, 3H).

15-HO-1-AG. [15(S)-Hydroxy-eicosa-5Z,8Z,11Z,13E-tetraenoic Acid 2,3(R)-Dihydroxypropyl Ester]. Soybean lipoxygenase: $^1\text{H NMR}$ (CDCl_3): δ 6.53 (dd, $J = 15.2$ Hz, 1H), 6.00 (t, $J = 11.2$ Hz, 1H), 5.70 (dd, $J = 6.5$ Hz, 1H), 5.40 (m, 5H), 4.19 (m, 2H), 3.92 (m, 1H), 3.67 (m, 2H), 2.97 (m, 2H), 2.82 (m, 2H), 2.37 (t, $J = 7.4$ Hz, 2H), 2.12 (m, 2H), 1.72 (q, $J = 7.3$ Hz, 2H), 1.55 (m, 2H), 1.35 (m, 6H), 0.89 (t, $J = 7.1$ Hz, 3H). NaBH_4 and H_2 reduced trimethyl silyl ether GC/MS m/z 618 [M^+], 603 [M^+-CH_3], 547 [$\text{M}^+-\text{C}_5\text{H}_{11}$], 173 [$\text{C}_6\text{H}_{11}\text{OTMS}^+$], 103 [CH_2OTMS^+], 73 [TMS^+].

15-HO-3-AG. [15(S)-Hydroxy-eicosa-5Z,8Z,11Z,13E-tetraenoic Acid 1,2(R)-Dihydroxypropyl Ester]. Soybean lipoxygenase: $^1\text{H NMR}$ (CDCl_3): δ 6.53 (dd, $J = 15.2$ Hz, 1H), 6.00 (t, $J = 11.1$ Hz, 1H), 5.70 (dd, $J = 6.4$ Hz, 1H), 5.40 (m, 5H), 4.19 (m, 2H), 3.92 (m, 1H), 3.65 (m, 2H), 2.97 (m, 2H), 2.82 (m, 2H), 2.37 (t, $J = 7.4$ Hz, 2H), 2.12 (m, 2H), 1.72 (q, $J = 7.3$ Hz, 2H), 1.55 (m, 2H), 1.35 (m, 6H), 0.89 (t, $J = 6.6$ Hz, 3H). NaBH_4 and H_2 reduced trimethyl silyl ether GC/MS m/z 618 [M^+], 603 [M^+-CH_3], 547 [$\text{M}^+-\text{C}_5\text{H}_{11}$], 173 [$\text{C}_6\text{H}_{11}\text{OTMS}^+$], 103 [CH_2OTMS^+], 73 [TMS^+].

Membrane Preparation for Binding Assay. Male Wistar rats (250–280 g) were maintained on a 12 h light/dark schedule. Food and water were ad libitum. The experimental protocol and procedures used met the guidelines of the Ministry of Health (G.U. No. 40, February 18, 1992) and were approved by the Animal Care Committee (University of Rome "Tor Vergata"). Rat forebrain and spleen membrane preparations were obtained using the method of Devane et al.⁴⁹ and were stored at a concentration of 1 mg mL^{-1} protein in 50 mM Tris-HCl, 2 mM Tris-EDTA, 3 mM MgCl_2 buffer, pH 7.4, at -80°C for no longer than 1 week. The protein concentration was determined using bovine serum albumin (BSA) as a standard.⁵⁰

CB Binding Assay. A rapid filtration assay was performed with [³H]-labeled CP-55,940, according to Compton et al.⁵¹ Incubations were performed in a final volume of 0.5 mL of 50 mM Tris·HCl, 2 mM Tris·EDTA, 3 mM MgCl₂, 5 mg mL⁻¹ BSA buffer, pH 7.4. PMSF (final concentration 50 μM) was added freshly each time just before the incubations started. The binding was initiated by the addition of 50 μg of protein of the membrane preparation and stopped after 1 h at 30 °C. The washed filters were transferred to vials, which contained 0.5 mL of 0.1% Triton X-100 and 3.5 mL of liquid scintillation cocktail (LSC) for nonaqueous solutions (Sigma Chemical Company). The vials were incubated overnight before counting. Unspecific binding was determined in the presence of 10 μM AEA. Binding data were elaborated through nonlinear regression analysis, using the Prism 3 program (GraphPAD Software for Science), and inhibition constants (*K_i*) were calculated. The following *K_d* values were calculated from [³H] CP-55,940 saturation curves of brain membrane preparations (*K_d* = 0.8 ± 0.2 nM) and of spleen membrane preparations (*K_d* = 0.2 ± 0.1 nM).

AEA Transporter Activity. The uptake of [³H]AEA by intact U937 cells was studied as described previously.⁵² Incubations (15 min) were carried out with different concentrations of [³H]AEA, in the range 0–1000 nM, to determine the kinetic constants, i.e., apparent Michaelis–Menten constant (*K_m*), maximum velocity (*V_{max}*), and inhibition constant (*K_i*) by nonlinear regression analysis through the Prism 3 program.⁵²

FAAH Activity. FAAH activity was assayed in U937 cells by measuring the release of [³H]arachidonic acid from [³H]-AEA using RP-HPLC as reported.⁴⁶ Kinetic studies were performed using different concentrations of [³H]AEA (in the range of 0–25 μM), and the kinetic constants (*K_m*, *V_{max}*, and *K_i*) were calculated by nonlinear regression analysis through the Prism 3 program.⁷

2D NMR. ¹H NMR spectra of 15-HETE were recorded at 500 MHz with a Bruker DRX-500 (Bijvoet Center for Biomolecular Research). Spectra were obtained at a probe temperatures 27 °C for D₂O (0.2 mmol L⁻¹; pH 6) and CDCl₃ (40 mmol L⁻¹) solutions and 4 °C for a CD₃OD (40 mmol L⁻¹) solution. Phase sensitive (States-TPPI) 2D NOESY, 2D off-resonance ROESY, and 2D TOCSY were recorded in addition to high-resolution 1D spectra. The 2D TOCSY spectrum was obtained using an MLEV-17 isotropic mixing sequence of 15 ms at a spin-lock field strength corresponding to 9.2 kHz. Two-dimensional NOESY spectra were obtained with an 800 ms mixing time. The 2D off-resonance ROESY spectrum in D₂O solution was recorded with an adiabatic spin-lock pulse of 350 ms at a field strength corresponding to 6.1 kHz. The spin-lock frequency was alternately placed 3520 Hz upfield or downfield of the center of the spectrum, thus obtaining an average spin-lock angle $\langle \vartheta \rangle = 60^\circ$. Chemical shifts for ¹H are expressed in ppm relative to internal TMS (0.0 ppm) for CDCl₃ solutions and relative to internal acetone (2.218 ppm) for D₂O solutions.

The chemical shift and scalar coupling values were extracted through direct measurement in the high-resolution 1D NMR spectra or through simulation of the more complex spectral regions. The assignment of the ¹H signals in the NMR spectra was obtained through combined analysis of the multiplet profiles in the 1D NMR spectra, and cross-peaks in the 2D TOCSY spectrum. The NOESY and off-resonance ROESY spectrum supplied Supporting Information to corroborate the assignments.

MD Calculations. MD simulations were performed using the GROMOS87 program package⁵³ on PCs running Linux. Each molecule was surrounded by SPC/E⁵⁴ water molecules in a truncated octahedron with periodic boundary conditions. All bond lengths were kept fixed using the SHAKE procedure.⁵⁵ Nonbonded interactions were calculated using the twin-range cutoff procedure with cutoff radii of 0.9 and 1.2 nm, and a time step of 2 fs was used. Simulations were performed with loose coupling to a pressure bath at 1 atm and a temperature bath at 300 K⁵⁶ with time constants of 0.5 and 0.1 ps,

respectively. Atom positions were restrained by applying a harmonic oscillator force constant of 10⁴ kcal mol⁻¹ Å⁻².

Description of Force Field Adaptions. A new atom type CS has been created to represent a bare sp³ carbon, which is in all aspects identical to CH1 and CH2, except for the van der Waals parameters that are identical to those of C or CB. To represent the double bonds, two new atom types, CEH1 and CIH1, have been created. CEH1 represents the C atoms involved in a double bond and the external C atoms of a conjugated double bond. CIH1 represents the internal C atoms of a conjugated double bond. These two new atom types are equivalent to the CR51 and CR61 atom types except for the parameters listed in the Supporting Information.

Acknowledgment. We thank B. Merghart for technical assistance and Dr. L. M. J. Kroon-Batenburg (Department of Crystal and Structural Chemistry, Utrecht University) for valuable discussions regarding the force field. Henk Obbink and Wim Lensing (Utrecht University research station “Tolakker”) are also acknowledged for their help.

Supporting Information Available: ¹H chemical shifts (500 MHz) of 15-HETE in D₂O and CDCl₃ and detailed force field parameter modifications.

References

- Di Marzo, V.; Melck, D.; Bisogno, T.; De Petrocellis, L. Endocannabinoids: endogenous cannabinoid receptor ligands with neuromodulatory action. *Trends Neurosci.* **1998**, *21*, 521–528.
- Pertwee, R. G. Pharmacology of cannabinoid CB1 and CB2 receptors. *Pharmacol. Ther.* **1997**, *74*, 129–180.
- Devane, W. A.; Hanus, L.; Breuer, A.; Pertwee, R. G.; Stevenson, L. A.; Griffin, G.; Gibson, D.; Mandelbaum, A.; Etinger, A.; Mechoulam, R. Isolation and structure of a brain constituent that binds to the cannabinoid receptor [see comments]. *Science* **1992**, *258*, 1946–1949.
- Mechoulam, R.; Ben-Shabat, S.; Hanus, L.; Ligumsky, M.; Kaminski, N. E.; Schatz, A. R.; Gopher, A.; Almag, S.; Martin, B. R.; Compton, D. R.; et al. Identification of an endogenous 2-monoglyceride, present in canine gut, that binds to cannabinoid receptors. *Biochem. Pharmacol.* **1995**, *50*, 83–90.
- Sugiura, T.; Kondo, S.; Sukagawa, A.; Nakane, S.; Shinoda, A.; Itoh, K.; Yamashita, A.; Waku, K. 2-Arachidonoylglycerol: a possible endogenous cannabinoid receptor ligand in brain. *Biochem. Biophys. Res. Commun.* **1995**, *215*, 89–97.
- Hillard, C. J.; Jarrahian, A. The movement of N-arachidonylethanolamine (anandamide) across cellular membranes. *Chem. Phys. Lipids.* **2000**, *108*, 123–134.
- Maccarrone, M.; van der Stelt, M.; Rossi, A.; Veldink, G. A.; Vliegthart, J. F.; Agro, A. F. Anandamide hydrolysis by human cells in culture and brain. *J. Biol. Chem.* **1998**, *273*, 32332–32339.
- Cravatt, B. F.; Giang, D. K.; Mayfield, S. P.; Boger, D. L.; Lerner, R. A.; Gilula, N. B. Molecular characterization of an enzyme that degrades neuromodulatory fatty-acid amides. *Nature* **1996**, *384*, 83–87.
- Di Marzo, V.; Goparaju, S. K.; Wang, L.; Liu, J.; Batkai, S.; Jarai, Z.; Fezza, F.; Miura, G. I.; Palmiter, R. D.; Sugiura, T.; Kunos, G. Leptin-regulated endocannabinoids are involved in maintaining food intake. *Nature* **2001**, *410*, 822–825.
- Maccarrone, M.; Valensise, H.; Bari, M.; Lazzarin, N.; Romanini, C.; Finazzi-Agro, A. Relation between decreased anandamide hydrolase concentrations in human lymphocytes and miscarriage [see comments]. *Lancet* **2000**, *355*, 1326–1329.
- Walker, J. M.; Huang, S. M.; Strangman, N. M.; Tsou, K.; Sanudo-Pena, M. C. Pain modulation by release of the endogenous cannabinoid anandamide. *Proc. Natl. Acad. Sci. U.S.A.* **1999**, *96*, 12198–12203.
- Wagner, J. A.; Varga, K.; Ellis, E. F.; Rzigalinski, B. A.; Martin, B. R.; Kunos, G. Activation of peripheral CB1 cannabinoid receptors in haemorrhagic shock. *Nature* **1997**, *390*, 518–521.
- van der Stelt, M.; Veldhuis, W. B.; Bar, P. R.; Veldink, G. A.; Vliegthart, J. F.; Nicolay, K. Neuroprotection by Delta9-tetrahydrocannabinol, the main active compound in marijuana, against ouabain-induced in vivo excitotoxicity. *J. Neurosci.* **2001**, *21*, 6475–6479.
- Piomelli, D.; Giuffrida, A.; Calignano, A.; Rodriguez de Fonseca, F. The endocannabinoid system as a target for therapeutic drugs. *Trends Pharmacol. Sci.* **2000**, *21*, 218–224.
- Giuffrida, A.; Beltramo, M.; Piomelli, D. Mechanisms of endocannabinoid inactivation: biochemistry and pharmacology. *J. Pharmacol. Exp. Ther.* **2001**, *298*, 7–14.

- (16) Baker, D.; Pryce, G.; Croxford, J. L.; Brown, P.; Pertwee, R. G.; Makriyannis, A.; Khanolkar, A.; Layward, L.; Fezza, F.; Bisogno, T.; Di Marzo, V. Endocannabinoids control spasticity in a multiple sclerosis model. *FASEB J.* **2001**, *15*, 300–302.
- (17) Kunos, G.; Jarai, Z.; Varga, K.; Liu, J.; Wang, L.; Wagner, J. A. Cardiovascular effects of endocannabinoids—the plot thickens. *Prostaglandins Other Lipid Mediators* **2000**, *61*, 71–84.
- (18) van der Stelt, M.; Veldhuis, W.; van Haften, G.; Fezza, F.; Bisogno, T.; Bär, P.; Veldink, G.; Vliegthart, J.; DiMarzo, V.; Nicolay, K. Exogenous anandamide protects rat brain against acute neuronal injury in vivo. *J. Neurosci.* **2001**, *21* (22), 8765–8771.
- (19) Panikashvili, D.; Simeonidou, C.; Ben-Shabat, S.; Hanus, L.; Breuer, A.; Mechoulam, R.; Shohami, E. An endogenous cannabinoid (2-AG) is neuroprotective after brain injury. *Nature* **2001**, *413*, 527–531.
- (20) Reggio, P. H.; Traore, H. Conformational requirements for endocannabinoid interaction with the cannabinoid receptors, the anandamide transporter and fatty acid amidohydrolase. *Chem. Phys. Lipids* **2000**, *108*, 15–35.
- (21) Khanolkar, A. D.; Palmer, S. L.; Makriyannis, A. Molecular probes for the cannabinoid receptors. *Chem. Phys. Lipids* **2000**, *108*, 37–52.
- (22) Porter, A. C.; Felder, C. C. The endocannabinoid nervous system. Unique opportunities for therapeutic intervention. *Pharmacol. Ther.* **2001**, *90*, 45–60.
- (23) Thomas, B. F.; Adams, I. B.; Mascarella, S. W.; Martin, B. R.; Razdan, R. K. Structure–activity analysis of anandamide analogues: relationship to a cannabinoid pharmacophore. *J. Med. Chem.* **1996**, *39*, 471–479.
- (24) Fichera, M.; Cruciani, G.; Bianchi, A.; Musumarra, G. A 3D-QSAR study on the structural requirements for binding to CB₁ (1) and CB₂ (2) cannabinoid receptors. *J. Med. Chem.* **2000**, *43*, 2300–2309.
- (25) Tong, W.; Collantes, E. R.; Welsh, W. J.; Berglund, B. A.; Howlett, A. C. Derivation of a pharmacophore model for anandamide using constrained conformational searching and comparative molecular field analysis. *J. Med. Chem.* **1998**, *41*, 4207–4215.
- (26) Shim, J. Y.; Welsh, W. J.; Cartier, E.; Edwards, J. L.; Howlett, A. C. Molecular interaction of the antagonist N-(piperidin-1-yl)-5-(4-chlorophenyl)-1-(2,4-dichlorophenyl)-4-methyl-1H-pyrazole-3-carboxamide with the CB₁ cannabinoid receptor. *J. Med. Chem.* **2002**, *45*, 1447–1459.
- (27) Edgemond, W. S.; Hillard, C. J.; Falck, J. R.; Kearn, C. S.; Campbell, W. B. Human platelets and polymorphonuclear leukocytes synthesize oxygenated derivatives of arachidonyl-ethanolamide (anandamide): their affinities for cannabinoid receptors and pathways of inactivation. *Mol. Pharmacol.* **1998**, *54*, 180–188.
- (28) Hampson, A. J.; Hill, W. A.; Zan-Phillips, M.; Makriyannis, A.; Leung, E.; Eglen, R. M.; Bornheim, L. M. Anandamide hydroxylation by brain lipoxygenase: metabolite structures and potencies at the cannabinoid receptor. *Biochim. Biophys. Acta* **1995**, *1259*, 173–179.
- (29) Sheskin, T.; Hanus, L.; Slager, J.; Vogel, Z.; Mechoulam, R. Structural requirements for binding of anandamide-type compounds to the brain cannabinoid receptor. *J. Med. Chem.* **1997**, *40*, 659–667.
- (30) Piomelli, D.; Beltramo, M.; Glasnapp, S.; Lin, S. Y.; Goutopoulos, A.; Xie, X. Q.; Makriyannis, A. Structural determinants for recognition and translocation by the anandamide transporter. *Proc. Natl. Acad. Sci. U.S.A.* **1999**, *96*, 5802–5807.
- (31) Hillard, C. J.; Edgemond, W. S.; Jarrhian, A.; Campbell, W. B. Accumulation of N-arachidonylethanolamine (anandamide) into cerebellar granule cells occurs via facilitated diffusion. *J. Neurochem.* **1997**, *69*, 631–638.
- (32) Boger, D. L.; Sato, H.; Lerner, A. E.; Hedrick, M. P.; Fecik, R. A.; Miyauchi, H.; Wilkie, G. D.; Austin, B. J.; Patricelli, M. P.; Cravatt, B. F. Exceptionally potent inhibitors of fatty acid amide hydrolase: the enzyme responsible for degradation of endogenous oleamide and anandamide. *Proc. Natl. Acad. Sci. U.S.A.* **2000**, *97*, 5044–5049.
- (33) Stella, N.; Schweitzer, P.; Piomelli, D. A second endogenous cannabinoid that modulates long-term potentiation. *Nature* **1997**, *388*, 773–778.
- (34) Ueda, N.; Yamamoto, K.; Yamamoto, S.; Tokunaga, T.; Shirakawa, E.; Shinkai, H.; Ogawa, M.; Sato, T.; Kudo, I.; Inoue, K.; et al. Lipoxygenase-catalyzed oxygenation of arachidonylethanolamide, a cannabinoid receptor agonist. *Biochim. Biophys. Acta* **1995**, *1254*, 127–134.
- (35) Moody, J. S.; Kozak, K. R.; Ji, C.; Marnett, L. J. Selective oxygenation of the endocannabinoid 2-arachidonylethanolamide by leukocyte-type 12-lipoxygenase. *Biochemistry* **2001**, *40*, 861–866.
- (36) Maccarrone, M.; Fiorucci, L.; Erba, F.; Bari, M.; Finazzi-Agro, A.; Ascoli, F. Human mast cells take up and hydrolyze anandamide under the control of 5-lipoxygenase and do not express cannabinoid receptors. *FEBS Lett.* **2000**, *468*, 176–180.
- (37) Ben-Shabat, S.; Frider, E.; Sheskin, T.; Tamiri, T.; Rhee, M. H.; Vogel, Z.; Bisogno, T.; De Petrocellis, L.; Di Marzo, V.; Mechoulam, R. An entourage effect: inactive endogenous fatty acid glycerol esters enhance 2-arachidonylethanolamide activity. *Eur. J. Pharmacol.* **1998**, *353*, 23–31.
- (38) Rabinovich, A. L.; Ripatti, P. O. On the conformational, physical properties and functions of polyunsaturated acyl chains. *Biochim. Biophys. Acta* **1991**, *1085*, 53–62.
- (39) Rich, M. R. Conformational analysis of arachidonic and related fatty acids using molecular dynamics simulations. *Biochim. Biophys. Acta* **1993**, *1178*, 87–96.
- (40) Barnett-Norris, J.; Guarnieri, F.; Hurst, D. P.; Reggio, P. H. Exploration of biologically relevant conformations of anandamide, 2-arachidonylethanolamide, and their analogues using conformational memories. *J. Med. Chem.* **1998**, *41*, 4861–4872.
- (41) Xie, X. Q.; Yang, D. P.; Melvin, L. S.; Makriyannis, A. Conformational analysis of the prototype nonclassical cannabinoid CP-47,497, using 2D NMR and computer molecular modeling. *J. Med. Chem.* **1994**, *37*, 1418–1426.
- (42) Reggio, P. H.; Greer, K. V.; Cox, S. M. The importance of the orientation of the C9 substituent to cannabinoid activity. *J. Med. Chem.* **1989**, *32*, 1630–1635.
- (43) Sugiura, T.; Kodaka, T.; Nakane, S.; Miyashita, T.; Kondo, S.; Suhara, Y.; Takayama, H.; Waku, K.; Seki, C.; Baba, N.; Ishima, Y. Evidence that the cannabinoid CB₁ receptor is a 2-arachidonylethanolamide receptor. Structure–activity relationship of 2-arachidonylethanolamide, ether-linked analogues, and related compounds. *J. Biol. Chem.* **1999**, *274*, 2794–2801.
- (44) van Zadelhoff, G.; Veldink, G. A.; Vliegthart, J. F. With anandamide as substrate plant 5-lipoxygenases behave like 11-lipoxygenases. *Biochem. Biophys. Res. Commun.* **1998**, *248*, 33–38.
- (45) van der Stelt, M.; Nieuwenhuizen, W. F.; Veldink, G. A.; Vliegthart, J. F. Dioxygenation of N-linoleoyl amides by soybean lipoxygenase-1. *FEBS Lett.* **1997**, *411*, 287–290.
- (46) van der Stelt, M.; Paoletti, A. M.; Maccarrone, M.; Nieuwenhuizen, W. F.; Bagetta, G.; Veldink, G. A.; Finazzi Agrò, A.; Vliegthart, J. F. G. The effect of hydroxylation of linoleoyl amides on their cannabinomimetic properties. *FEBS Lett.* **1997**, *415*, 313–316.
- (47) Ueda, N.; Yamamoto, K.; Kurahashi, Y.; Yamamoto, S.; Ogawa, M.; Matsuki, N.; Kudo, I.; Shinkai, H.; Shirakawa, E.; Tokunaga, T. Oxygenation of arachidonylethanolamide (anandamide) by lipoxygenases. *Adv. Prostaglandin Thromboxane Leukot. Res.* **1995**, *23*, 163–165.
- (48) Van der Stelt, M.; Noordermeer, M. A.; Kiss, T.; Van Zadelhoff, G.; Merghart, B.; Veldink, G. A.; Vliegthart, J. F. G. Formation of a new class of oxylipins from N-acyl(ethanol)amines by the lipoxygenase pathway. *Eur. J. Biochem.* **2000**, *267*, 2000–2007.
- (49) Devane, W. A.; Dysarz, F. A. d.; Johnson, M. R.; Melvin, L. S.; Howlett, A. C. Determination and characterization of a cannabinoid receptor in rat brain. *Mol. Pharmacol.* **1988**, *34*, 605–613.
- (50) Bradford, M. M. A rapid and sensitive method for the quantitation of microgram quantities of protein utilizing the principle of protein-dye binding. *Anal. Biochem.* **1976**, *72*, 248–254.
- (51) Compton, D. R.; Rice, K. C.; De Costa, B. R.; Razdan, R. K.; Melvin, L. S.; Johnson, M. R.; Martin, B. R. Cannabinoid structure–activity relationships: correlation of receptor binding and in vivo activities. *J. Pharmacol. Exp. Ther.* **1993**, *265*, 218–226.
- (52) Maccarrone, M.; Bari, M.; Lorenzon, T.; Bisogno, T.; Di Marzo, V.; Finazzi-Agro, A. Anandamide uptake by human endothelial cells and its regulation by nitric oxide. *J. Biol. Chem.* **2000**, *275*, 13484–13492.
- (53) van Gunsteren, W. F.; Berendsen, H. J. C. *GROMOS-87: Groningen Molecular Simulation Program Package*; Groningen, The Netherlands, 1987.
- (54) Berendsen, H. J. C.; Grigera, J. R.; Straatsma, T. P. The missing term in effective pair potentials. *J. Phys. Chem.* **1987**, *91*, 6269–6271.
- (55) Ryckaert, J. P.; Gicco, G.; Berendsen, H. J. C. Numerical integration of the Cartesian equation of motion of a system with constraints: molecular dynamics of N-alkanes. *J. Comput. Phys.* **1987**, *23*, 327–341.
- (56) Berendsen, H. J. C.; Postma, J. P. M.; van Gunsteren, W. F.; Di Niola, A.; Haak, J. R. Molecular dynamics with coupling to an external bath. *J. Chem. Phys.* **1984**, *81*, 3684–3690.